The Journal of Experimental Biology 208, 2377-2387
Published by The Company of Biologists 2005
doi:10.1242/jeb.01618

Patterns of red muscle strain/activation and body kinematics during steady swimming in a lamnid shark, the shortfin mako (*Isurus oxyrinchus*)

Jeanine M. Donley[1,*], Robert E. Shadwick[1], Chugey A. Sepulveda[2], Peter Konstantinidis[3] and Sven Gemballa[3]

[1]*Marine Biology Research Division, Scripps Institution of Oceanography, University of California, San Diego, La Jolla, CA 92093-0202, USA,* [2]*Pfleger Institute of Environmental Research, Oceanside, CA 92054, USA* and [3]*Department of Zoology, University of Tübingen, Auf der Morgenstelle 28, 72076 Tübingen, Germany*

*Author for correspondence (e-mail: jdonley@ucsd.edu)

Accepted 29 March 2005

Summary

The dynamics of steady swimming were examined in the shortfin mako (*Isurus oxyrinchus*), a member of the cartilaginous fish family Lamnidae, a family known for their morphological adaptations for high-performance locomotion and their similarity in hydromechanical design to tunas. Patterns of red muscle (RM) strain (i.e. relative length change) and activation were quantified at two axial positions (~0.4 and 0.6*L*, where *L* is total body length), using sonomicrometry and electromyography (EMG), and correlated with simultaneous measurements of dorsal midline kinematics during steady swimming (~0.5–1 *L* s^{-1}). RM strain varied longitudinally with strain amplitudes ranging from 5.5±1.1% (S.E.M.) in the anterior to 8.7±0.9% in the posterior. We found no significant longitudinal variation in patterns of RM activation, with mean onset of activation occurring at 83–84° (90° is peak length) and offset at 200–210° at both body positions. Likewise, duty cycles were similar: 35.5±1.0% in the anterior and 32.2±1.6% in the posterior. Comparison of the timing of waves of dorsal midline curvature and predicted strain relative to measured RM strain revealed a phase shift between RM shortening and local body bending. Furthermore, when the body is bent passively, RM shortens synchronously with the surrounding white muscle (WM) and skin, as expected. During active swimming, peaks in RM strain were delayed relative to peaks in WM strain by a mean of ~10% of the tailbeat cycle, with one individual as high as ~17% in the anterior and nearly 50% in the posterior. The longitudinal consistency in the EMG/strain phase relationship in the mako is similar to that in the leopard shark, suggesting a consistent trend among sharks using different locomotor modes. However, unlike in the leopard shark, RM shortening in the mako is physically uncoupled from deformation of the surrounding body during steady swimming, a characteristic shared between the mako and tunas.

Key words: muscle activation, strain, swimming, lamnid, *Isurus*.

Introduction

Previous studies have examined the role of skeletal muscle in the mechanics of steady swimming of a number of bony fish species (reviewed in Altringham and Ellerby, 1999; Coughlin, 2002). Specifically, temporal patterns of red muscle (RM) shortening and activation recorded during swimming bouts have been used to infer functional properties of the RM along the body (Williams et al., 1989; van Leeuwen et al., 1990; Rome et al., 1993; Wardle and Videler, 1993; Jayne and Lauder, 1995b; Gillis, 1998; Hammond et al., 1998; Shadwick et al., 1998; Ellerby and Altringham, 2001; Knower et al., 1999). These studies have revealed a striking trend in that dynamic muscle function varies along the body in fishes across a wide range of taxa. For example, most bony fish species examined display some degree of longitudinal variation in the phase of RM activation, typically consisting of a rostrocaudal negative phase shift in the onset of muscle activation [measured by electromyography (EMG)] relative to the muscle strain cycle, and a decrease in the duration of muscle activation in more posterior regions of the body (Williams et al., 1989; van Leeuwen et al., 1990; Rome et al., 1993; Wardle and Videler, 1993; Jayne and Lauder 1995b; Gillis, 1998; Hammond et al., 1998; Shadwick et al., 1998; Knower et al., 1999; Ellerby and Altringham, 2001). Thus, different species may generate variable patterns of muscle activation and strain in order to optimize regional muscle function and power output along the body for their particular swimming mode, such as cruising or maneuvering (Wardle et al., 1995), or even for the physical properties of the fluid medium (Biewener and Gillis, 1999).

Considering the amount of interest in the swimming mechanics of fishes, it is surprising that few studies have examined dynamic muscle function in elasmobranchs. In a

previous study, we found that the leopard shark (*Triakis semifasciata*), a common temperate subcarangiform swimmer, lacks longitudinal variation in the timing of RM activation with respect to muscle strain (Donley and Shadwick, 2003). These findings are in contrast with values reported for most bony fishes and have fueled hypotheses regarding the evolution of muscle mechanical design in these two distantly related groups of fishes.

As in bony fishes, sharks also display a broad spectrum of swimming modes, ranging from species with a high degree of lateral undulation (such as the leopard shark) to more tuna-like species such as the lamnid sharks (Family Lamnidae) (Donley et al., 2004). The present study examines steady-swimming kinematics and muscle dynamics in a lamnid shark, the shortfin mako (*Isurus oxyrinchus*). Furthermore, it considers specific aspects of the morphological relationship between the RM and intermuscular tendons. Specific objectives are to (1) examine longitudinal patterns of RM activation and strain in the mako during steady swimming and clarify modes of transmission of muscular forces along intermuscular tendons, (2) quantify patterns of body curvature and lateral displacement derived from analysis of the swimming kinematics and (3) compare these results with kinematic and muscle dynamic characteristics investigated previously in the leopard shark to test the hypothesis that the lack of longitudinal variation in the EMG/strain phase relationship is a characteristic consistent among sharks that utilize different modes of body/caudal fin propulsion.

Materials and methods

Experimental subjects and protocol

Experiments on the shortfin mako (*Isurus oxyrinchus* R.) were conducted at the Scripps Institution of Oceanography (SIO). Makos ranging in size from 80 to 112 cm total body length (*L*) (~3.5–10.6 kg) were collected by hook and line off the coast of Southern California and transported back to the laboratory facilities. Once at SIO, the sharks were placed into a velocity-controlled 3000-liter swim tunnel (described in Graham et al., 1990) and allowed to acclimate to the test chamber prior to experimentation. All procedures followed the guidelines of the University of California Animal Care Protocol. Due to the difficulties associated with locating, capturing and handling these pelagic sharks, it took two years to successfully complete experiments on 10 individuals.

Sonomicrometry and electromyography

Surgery was performed on anesthetized individuals (0.0028 g l^{-1} ethyl p-aminobenzoate) partially submerged in a seawater bath to implant precalibrated piezoelectric crystals and EMG electrodes for *in vivo* detection of instantaneous muscle segment length changes (strain) and activation patterns (as described in Shadwick et al., 1999; Donley and Shadwick, 2003) (Fig. 1). The two axial positions (0.4±0.02*L*, anterior; 0.6±0.04*L*, posterior) chosen for this study encompass much of the longitudinal distribution of RM in the mako (Bernal et al., 2003). Anterior to 0.35*L* and posterior to 0.65*L*, the mass of red muscle (RM) is relatively small and therefore the accuracy in crystal placement declined when attempting to implant crystals more rostral or caudal to these positions. To implant the crystals, a 2-mm incision was made in the skin directly dorsal to the desired region of the muscle and a puncture was made in the underlying tissue using a 15-gauge hypodermic needle precalibrated to the required depth. Crystals were implanted in a longitudinal orientation approximately 15 mm apart such that the degree of shortening and lengthening of myotomes could be measured. This orientation prevented the bending movements of the shark from causing slippage of the crystals within the muscle and avoided damaging the lateral vascular rete.

Pairs of EMG electrodes were implanted into the RM approximately 2 mm apart, directly bisecting each

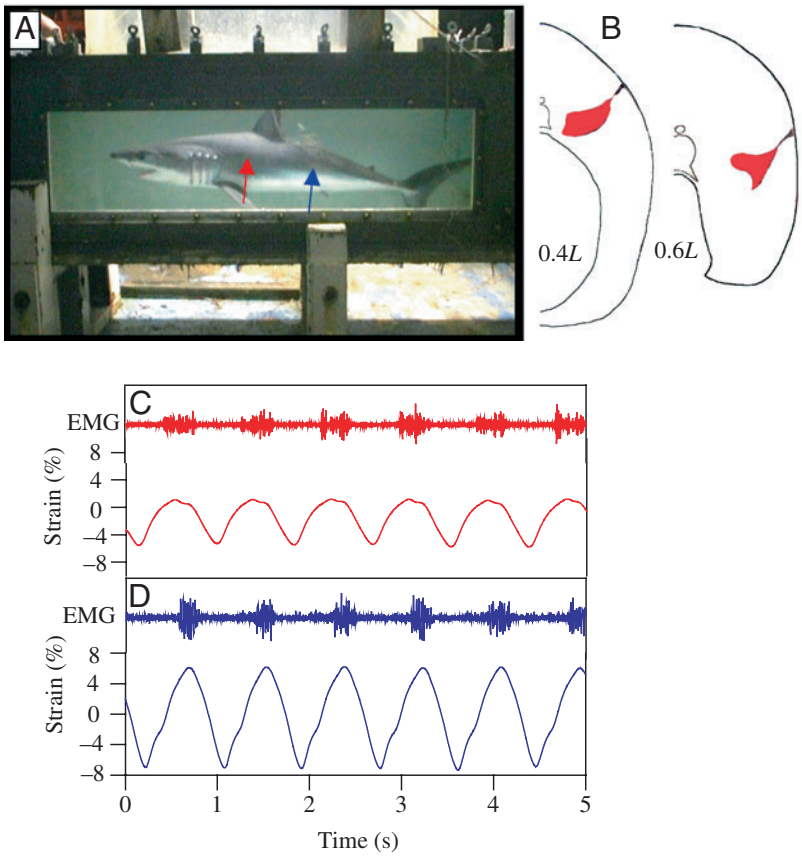

Fig. 1. Sample sonomicrometric and electromyogram (EMG) traces from swimming *I. oxyrinchus*. (A) Lateral view of a 91 cm mako swimming at ~1 *L* s^{-1} in the swim tunnel. Red and blue arrows correspond to the axial positions shown in B–D. (B) Mako cross sections at 0.4 and 0.6*L*, showing the difference in size and location of the red muscle mass at the two axial positions. Sample of EMG and sonomicrometric data recorded simultaneously over several consecutive tailbeat cycles in the anterior (C) and posterior (D) axial positions.

Table 1. *Mean muscle strain and activation phase in* I. oxyrinchus *swimming at ~0.5* L s^{-1}

Body position	Strain (%)	EMG onset (deg.)	EMG offset (deg.)	Duty cycle (%)
0.40±0.015*L*	±5.5±1.1 (8)	84.2±1.2 (7)	210.8±3.6 (7)	35.5±1.0 (7)
0.60±0.038*L*	±8.7±0.9 (7)	83.9±1.3 (7)	199.7±5.5 (7)	32.2±1.6 (7)

Values are means ± S.E.M.; sample sizes are in parentheses.

sonomicrometric crystal pair (all sonomicrometry measurements were coupled with EMG recordings). Wires were anchored to the skin with sutures. Following surgery, the fish were placed into the swim tunnel and allowed to recover prior to data collection. EMG signals were amplified using A.C. preamplifiers (Grass Instrument Co., West Warwick, RT, USA; model P55), band pass filtered (3–300 Hz) and recorded simultaneously with the sonomicrometric data at 500 Hz during periods when the shark swam in the center of the flow chamber. Sonomicrometric and EMG data were filtered in AcqKnowledge 3.5 (Biopac Systems Inc., Santa Barbara, CA, USA) using a Blackman-92 dB FIR 60 Hz band stop filter to remove the electrical noise produced by the swim tunnel motor. EMG data were subject to an additional high pass filter (cut-off frequency of 3 Hz) to remove remaining low-frequency movement artifact. With a sample frequency of 500 Hz and a tailbeat frequency of 1 Hz, the error in EMG timing did not exceed 2 ms (an error of 0.2% of a cycle). At the end of each experiment, crystal and electrode position and body width at implantation sites were verified during *postmortem* dissection.

Crystal pairs and EMG electrodes were implanted into the deep RM at anterior and posterior axial positions (N=6). Furthermore, six additional experiments were performed in which a third set of sonomicrometric crystals was implanted in the white muscle (WM) adjacent to and at the same depth as a pair of crystals in the RM (N=3 for anterior; N=3 for posterior) to assess the degree of shearing between the RM and surrounding WM. To identify any differences in the amount of strain within the RM mass at a given body position, we also implanted two pairs of sonomicrometric crystals at the same posterior axial position within the RM, one pair located more medially and the other more peripherally within the RM mass. At the same axial position, a third pair was implanted into the WM. During the recovery period following surgery, we recorded muscle length changes during passive simulated swimming movements induced by gentle side-to-side motion of the center of mass that generated body undulation. After the sharks had completely recovered from the anesthesia, muscle dynamics were recorded during active steady swimming while sharks swam at speeds of ~0.5–1.0 L s^{-1}.

For each individual, muscle strain was calculated for 25–50 tailbeat cycles. Amplitudes represent the difference between peak and mean muscle segment length divided by mean segment length. The muscle strain waveform was periodic and therefore the phase of the strain cycle was designated in degrees (from 0 to 360) as described in Altringham and Johnston (1990). In AcqKnowledge, a voltage threshold was set to determine the timing of onset and offset of activation of the EMG bursts with precision over multiple tailbeat cycles (see Knower et al., 1999). The temporal relationships between the onset and offset of activation and muscle strain were expressed in degrees of the tailbeat cycle (0° is mean muscle length during lengthening, 90° is peak length). Duty cycle (expressed in both degrees and as a percentage of the strain cycle period) was calculated as the duration of EMG activity relative to the total duration of the strain cycle. EMG/strain phase and duty cycles are presented as an average of 25–50 tailbeat cycles for each fish. A sample data set from one individual, illustrating the sonomicrometric and EMG data common to all fish, is provided in Fig. 1. RM strain amplitudes are presented for eight individuals for the anterior position and for seven individuals for the posterior position. EMG data for both axial positions are presented for seven individuals.

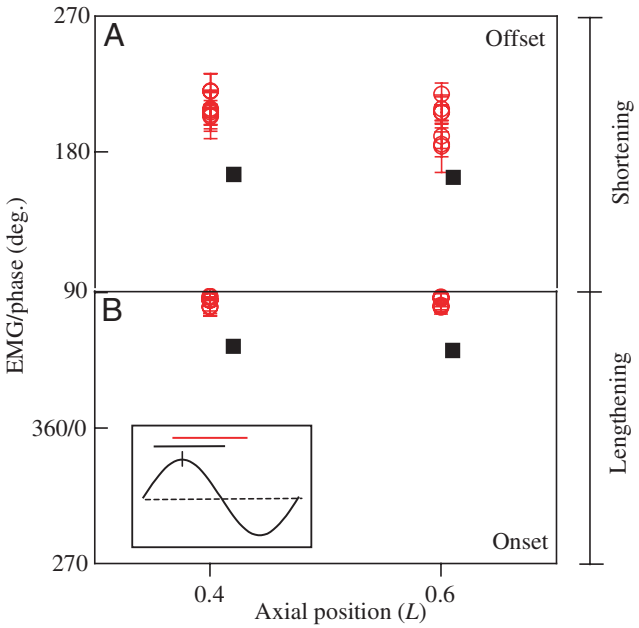

Fig. 2. Timing of electromyogram (EMG) offset (A) and onset (B) of activation relative to the strain cycle in all makos (N=7; open symbols) at anterior and posterior body positions, illustrating the lack of longitudinal variation in the phase of activation. Values shown for each individual represent a mean (±S.E.M.) of multiple tailbeat cycles. Also shown are mean EMG/strain phases for the leopard shark (filled symbols), modified from Donley and Shadwick (2003). Inset in B is a diagrammatic representation of activation phase relative to sinusoidal strain cycle in mako (red) and leopard shark (black).

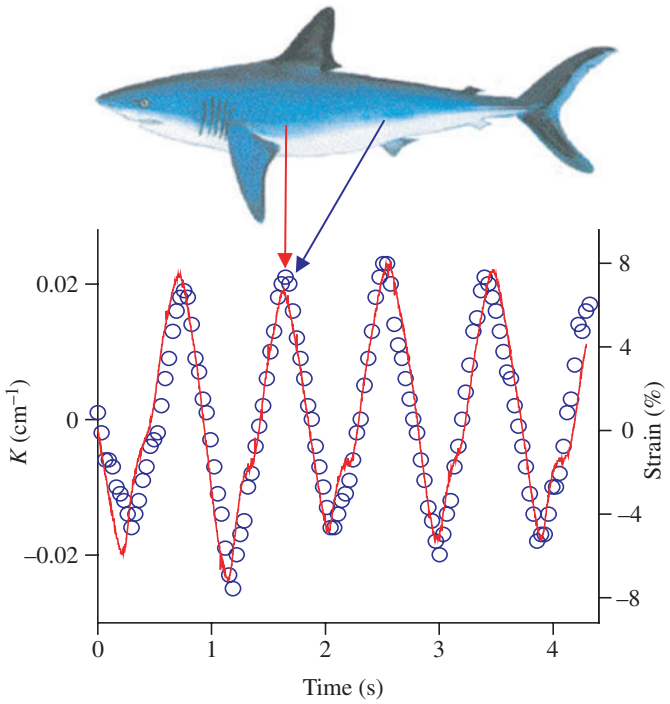

Fig. 3. Anterior red muscle strain (red trace), measured by sonomicrometry, superimposed onto predicted strain (open circles), calculated from midline curvature (K) at ~0.6L for four consecutive tailbeat cycles in an 80 cm mako. Red muscle strain at ~0.4L was in phase with curvature and predicted strain at ~0.6L. The mako image, modified from Compagno (1998), is used to illustrate the relative positions of synchronized strain and body curvature.

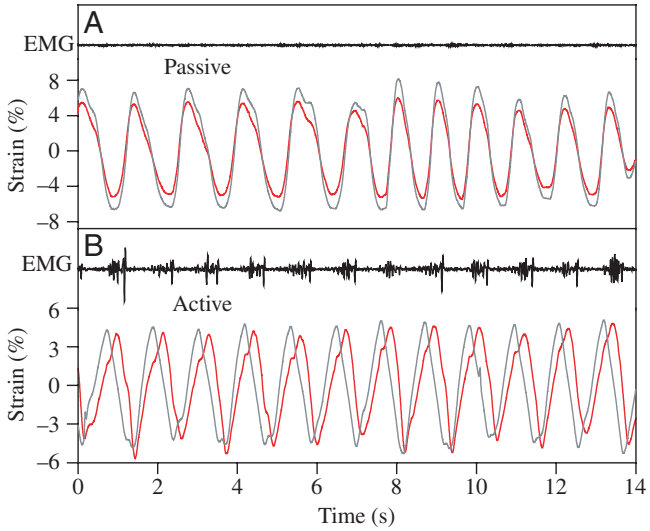

Fig. 4. Simultaneous recordings of red muscle (red trace) and adjacent white muscle (gray trace) strain at 0.4L during passive simulated swimming movements (A) and active steady swimming (0.5 L s^{-1}) (B) in *I. oxyrinchus*.

Kinematics

Kinematic analyses were performed on five individuals to calculate lateral displacement (D) and curvature (K) along the body during steady swimming. Video segments in which the fish completed four or more symmetrical tailbeat cycles swimming at ~1 Hz near the center of the swim chamber and corresponding to acceptable strain and EMG data were selected for analysis. To synchronize the video fields with the corresponding muscle strain and activation data, a flashing red diode was recorded in the video sequences, and its excitation voltage was recorded with the sonomicrometric and EMG data. A scaling factor was calculated for each video sequence using a 10-cm grid on the bottom of the swim chamber. A correction factor was calculated by comparing the known distance between two landmark points on the body of each individual with that distance measured in the video fields. Methods for video analysis were adapted from Jayne and Lauder (1995). Sequential video fields were digitized with 32 points along the dorsal outline, beginning anteriorly at the trailing edge of the pectorals (~0.3L) and ending at the tip of the caudal fin. A cubic spline function was used to convert the point coordinate data of each digitized outline into complete curves. A dorsal midline for each field was then calculated and divided into 50 equally spaced segments. At the intersection of each of these segments along the midline are the coordinate points used to calculate lateral displacement, defined as the progression of these points in the y-direction (perpendicular to axis of progression of the fish) and expressed as a percentage of L.

Curvature was calculated as described in previous studies (van Leeuwen et al., 1990; Rome et al., 1992; Coughlin et al., 1996; Katz and Shadwick, 1998; Donley and Shadwick, 2003). Midline coordinate data were normalized in the x-direction (defined by the direction of travel), and a fourth-order polynomial equation was fit to each midline (see Katz and Shadwick, 1998). K was calculated from the polynomial equations for numerous positions along the dorsal midline, including those corresponding to the sites of implanted crystals and electrodes; a positive value corresponds to lengthening of the muscle on the left side of the body (i.e. convex to the left). Predicted strain values were calculated by multiplying K at each body position in each field by the distance between the crystals and the center of the axis of bending (i.e. the vertebral column). A cross-correlation analysis was performed using DaDisp Version 4.0 (DSP Corp., Newton, MA, USA) to determine the relative phase shift between simultaneous waveforms of measured and predicted RM strain, as well as between measured RM and WM strain, at a given body position. Once the phase shift was determined, a correlation analysis was performed using the optimal phase shift to calculate a correlation coefficient (r^2 value). A cross-correlation analysis was also used to calculate the propagation speed of the wave of body curvature.

Propulsive wave velocity (C), the speed of the wave of lateral motion that travels along the body from snout to tail, was calculated by dividing the distance between the anterior and posterior positions by the time it took for the wave of lateral displacement to travel between these two points on the body. Propulsive wavelength (λ) was calculated by dividing C by mean tailbeat frequency.

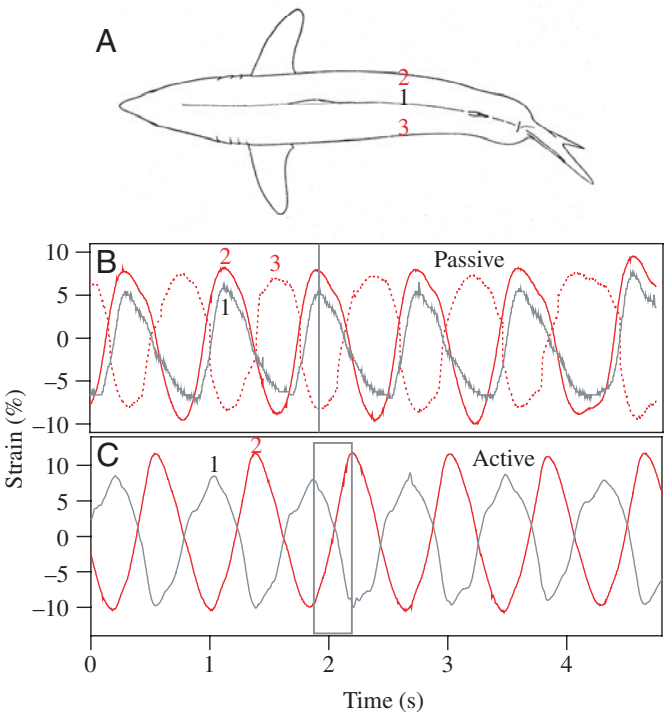

Fig. 5. Simultaneous recordings of red muscle (RM; red traces) and white muscle (WM; gray traces) strain at 0.6*L* on the right and left sides of the body during passive and active swimming in the mako. Numbers in A represent locations of implanted sonomicrometric crystals (1, WM near backbone on right side of the body; 2, RM on right side; 3, RM on left side). During passive simulated swimming movements (B), shortening in the red and white muscle on the right side of the body are in phase but 180° out of phase with shortening on the left side (vertical line), as expected. During active swimming (C), shortening in WM precedes shortening in RM by nearly 50% of the tailbeat cycle (box).

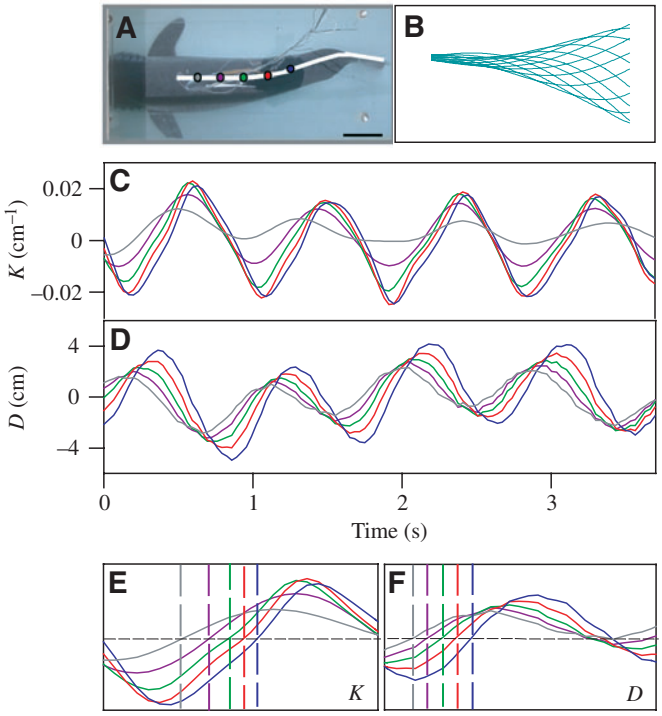

Fig. 6. Dorsal midline curvature (*K*) and lateral displacement (*D*) calculated at five axial positions (0.4, 0.5, 0.6, 0.7 and 0.8*L*: positions shown in A) for multiple consecutive complete tailbeat cycles. To illustrate the degree of lateral motion along the body during steady swimming, the dorsal midline through one tailbeat cycle is shown in B. Colors for each data trace in C–F correspond to the axial positions indicated in A. Scale bar, 8 cm. One tailbeat cycle is magnified to show the difference in the rates of propagation of the waves of curvature (E) and lateral displacement (F) along the body.

Statistical analyses

To address the question of whether there was a significant difference in RM strain, timing of EMG onset and offset, or duty cycle at the two body positions, a two-sample *t*-test (Knower et al., 1999) was performed (Minitab version 13.32) on each variable using a significance level of P=0.05.

Morphology

Microdissections of a cleared and stained specimen and standard histological techniques (20 µm; Azan-Domagk staining; Gemballa et al., 2003) were employed to characterize the position and trajectory of the hypaxial lateral tendon within the red and white musculature. Details of the techniques were described previously (Donley et al., 2004; Gemballa et al., 2003).

Results

In vivo *muscle shortening and activation patterns*

Steady-swimming muscle dynamics were examined in the shortfin mako swimming at sustained preferred cruising speeds of ~0.5–1.0 $L\ s^{-1}$; Table 1). Red muscle (RM) strain amplitudes in the anterior body position ranged from ±2.4 to ±9.5% among all individuals (N=8), with a mean amplitude of ±5.5%. Strain amplitudes in the posterior position ranged from ±6.6 to ±12.7% (N=7), with a mean amplitude of ±8.7%. Not all fish had a significant difference in strain at the two body positions; however, mean strain was generally higher in the posterior.

During each tailbeat cycle, the wave of activation traveled posteriorly along the body such that the posterior musculature was activated later in time than the anterior musculature (Fig. 1), as is typical in other fishes (Grillner and Kashin, 1976; Williams et al., 1989; He et al., 1990; van Leeuwen et al., 1990; Jayne and Lauder, 1993, 1995b; Gillis, 1998; Knower et al., 1999; Shadwick et al., 1999). When EMG timing was expressed in terms of the phase of local muscle strain, we found that, at both axial positions, activation began during muscle lengthening close to peak length and ended late in muscle shortening (Fig. 2). Specifically, in the anterior EMG, onset ranged from 80.3 to 87.5° (mean=84.2±1.2°, N=7) and offset occurred between 203.3 and 220.0° (mean=210.8±3.6°, N=7) (Table 1). At the posterior position, EMG onset ranged from 80.6 to 87.0° (mean=83.9±1.3°, N=7), while offset

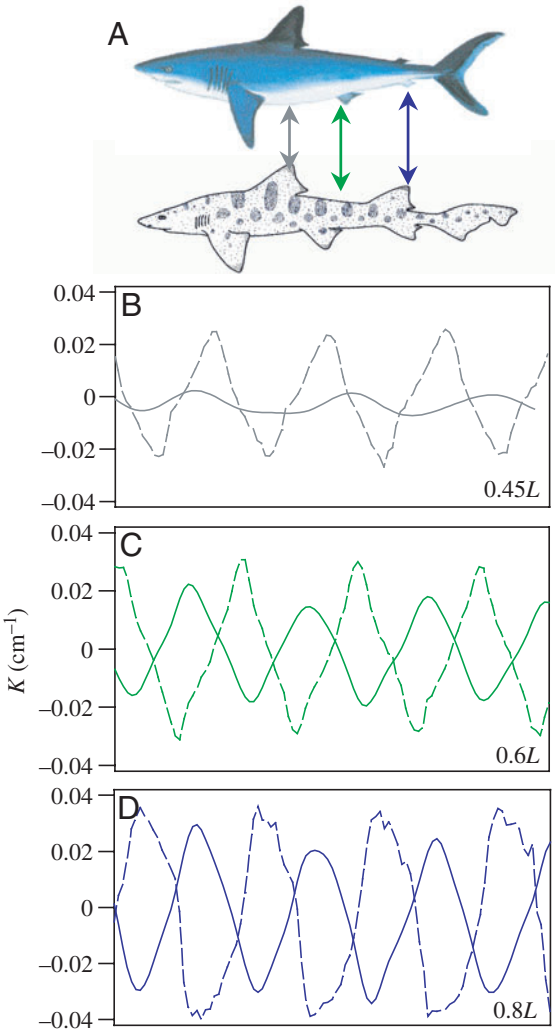

Fig. 7. Dorsal midline curvature as a function of time for several consecutive tailbeat cycles in the mako (solid lines) and leopard shark (broken lines; data from Donley and Shadwick, 2003). Data are presented for three body positions, as indicated by arrows in A: (B) 0.45*L*, (C) 0.6*L* and (D) 0.8*L*.

occurred between 183.4 and 208.3° (mean=199.7±5.5°, *N*=7). Mean duty cycle, expressed in degrees of the strain cycle, ranged from 124±3.3° in the anterior to 111±5.0° in the posterior. Given as a percentage of the tailbeat cycle, duty cycles were 35.5±1.0% in the anterior and 32.2±1.6% in the posterior (Table 1).

Relative to the phase of local muscle strain, there was no statistically significant difference in the EMG onset timing (*P*=0.782), offset timing (*P*=0.063) or duty cycle (*P*=0.073) at the two axial positions.

Muscle and body kinematics

Curvature (*K*) and lateral displacement (*D*) were calculated for several axial positions along the dorsal midline from video images of steady-swimming bouts. Predicted muscle strain was calculated from curvature for sites corresponding to those where muscle segment length recordings were made. In all individuals, the peaks in predicted strain (and curvature) preceded (in time) the peaks in measured RM strain (*N*=5). Amplitudes of predicted and measured RM strain were similar, with predicted strain values of approximately ±7% in the anterior and ±9% in the posterior. Phase shifts of curvature relative to measured RM strain ranged from 58 to 64 ms, with a mean of 60.5 ms, corresponding to ~8% of the tailbeat cycle period. RM is therefore uncoupled from local body curvature and shortens in phase with curvature at more posterior locations, as illustrated in Fig. 3, where RM strain at 0.42*L* occurred in synchrony with midline curvature at 0.6*L*. As a direct measure of the degree of uncoupling that can occur between active RM and inactive WM, we compared timing of RM and WM strain waveforms at 0.4*L* during simulated and active swimming. During passive simulated swimming movements induced under anesthesia, in which all muscle was inactive, length changes in RM and adjacent WM were closely matched in phase (Fig. 4A), as one would expect. However, during steady swimming using only RM, the waveforms were no longer synchronized; WM strain preceded (in time) the peak in RM strain (Fig. 4B). By cross-correlation analysis, we determined that the mean phase shift between simultaneous recordings of RM and WM strain was 90 ms [or ~10% of the tailbeat cycle, with one individual as high as 174 ms (~17%)]. r^2 values for these correlations ranged from 0.892 to 0.977.

The phase relationship between local shortening in RM and WM during passive and active swimming was also examined in the posterior body position. Fig. 5 illustrates an experiment where crystals were placed in the RM and adjacent WM on the right side of the body directly opposite a pair of crystals implanted in the RM on the left side (Fig. 5A). During passive simulated swimming, shortening in the posterior WM and RM (1 and 2, respectively, in Fig. 5) were in phase on the right side of the body and 180° out of phase with shortening of the RM on the left side of the body, as expected (Fig. 5B), but during active swimming (Fig. 5C), shortening in the WM preceded that in RM by a mean of 248 ms (~48% of the tailbeat cycle), a substantially greater phase shift than in the anterior position.

Comparison of curvature calculated for several positions along the dorsal midline between 0.4 and 0.8*L* indicates that both the amplitude of curvature as well as the speed of progression of the wave of curvature increases posteriorly (Figs 6, 7). Between 0.4 and 0.6*L*, the speed of propagation of the wave of midline curvature ranged from 240 to 1332 $L\ s^{-1}$ among five makos (Table 2). Amplitudes of lateral displacement also increased posteriorly, ranging from 1.33±0.10% at 0.38*L* to 12.94±0.86% at 1.0*L*. The speed of progression of the wave of lateral displacement (propulsive wave velocity) remained constant from snout to tail and ranged between 138 and 170 $cm\ s^{-1}$ (1.6–1.8 $L\ s^{-1}$) (Fig. 6; Table 2). Because of the lack of a phase shift in timing of muscle activation from anterior to posterior, the speed of the wave of muscle contraction from anterior to posterior is the same as the propulsive wave velocity (Table 2). Propulsive wavelengths were between 152 and 175 cm in makos of lengths 80 to 92.3 cm, or 1.8 to 2.1*L* (Table 2).

Table 2. *Kinematic parameters calculated from analysis of dorsal video footage in steady swimming* I. oxyrinchus

L (cm)	*C* (cm s^{-1})	*C* (*L* s^{-1})	λ (*L*$^{-1}$)	tbf (Hz)	Strain wave velocity (*L* s^{-1})	*K* wave velocity (*L* s^{-1})
92.3	169.7	1.8	1.9	0.98	1.8	14.4
80.0	147.9	1.8	2.1	0.89	1.4	4.6
88.0	152.1	1.7	2.0	0.87	–	2.7
81.1	143.2	1.8	2.1	0.85	1.8	6.3
84.4	138.2	1.6	1.8	0.90	1.4	14.7

L, total body length; *C*, propulsive wave velocity; λ, propulsive wavelength; tbf, tailbeat frequency; *K*, curvature.

To test whether the amplitude of strain varies within the RM mass at one axial position, an additional experiment was performed in which two pairs of sonomicrometric crystals were placed at the same posterior axial position within the RM, one pair located more medially and the other more peripherally within the RM mass, and a third pair in the adjacent WM (Fig. 8A). Strain amplitudes and phases varied within the RM mass. Strain was greater near the lateral surface of the RM mass. Furthermore, peaks in WM strain (1 in Fig. 8B) preceded peaks in medial RM strain (3 in Fig. 8B) by nearly 50% of the strain cycle in this posterior position but were in phase with shortening in the peripheral RM (2 in Fig. 8B).

Discussion

Patterns of muscle shortening

Mako RM strain amplitudes, as well as the trend for strain to increase from anterior (~0.4*L*) to posterior (~0.6*L*), were consistent with observations in teleosts such as saithe (Hess and Videler, 1984), carp (van Leeuwen et al., 1990), scup (Rome et al., 1990, 1993; Coughlin and Rome, 1996), trout (Hammond et al., 1998; Coughlin, 2000), mackerel (Shadwick et al., 1998) and bonito (Ellerby et al., 2000). Overall, mean amplitudes were ±5.5% in the anterior and ±8.7% in the posterior. Using similar methods, Donley and Shadwick (2003) reported RM strain amplitudes of ±3.9% at 0.4*L* and ±6.6% at 0.6*L* in leopard sharks swimming at comparable speeds (~1 *L* s^{-1}). At both axial positions, muscle strain was greater in the mako than in the leopard shark, even though midline curvature of the mako was lower (Fig. 7) and its RM is much closer to the vertebral column, where strain would be substantially reduced if the body deformed as a simple beam (Katz et al., 1999). Likewise, the deep RM in skipjack and yellowfin tunas typically undergoes strains of ±5 to 8% between axial positions of 0.4 and 0.65*L* (Shadwick et al., 1999), which is as great or greater than strain in superficial RM of other swimming teleosts (Hammond et al., 1998; Hess and Videler, 1984; van Leeuwen et al., 1990; Rome and Swank, 1992; Rome et al., 1993; Shadwick et al., 1998; Ellerby et al., 2000). RM strain predicted from beam theory was comparable to measured values and averaged ~7% in the anterior and 9% in the posterior in the mako. Tuna, by contrast, have measured strains that are twice the values predicted by beam theory (Katz et al., 2001). Although the mako and leopard sharks differ in terms of the placement of their RM relative to the vertebral column, the greater body thickness, and thus absolute distance, of the RM from the neutral axis of bending in the mako contributes to its greater overall (measured and predicted) strains. As in tunas, RM shortening is not directly linked to local body bending in the mako. Amplitudes of strain in internal RM in the mako are therefore not constrained by the distance from the backbone.

Amplitudes and phases of strain varied significantly within the RM mass at a given body position (Fig. 8). We found significantly lower strain amplitudes near the medial surface of

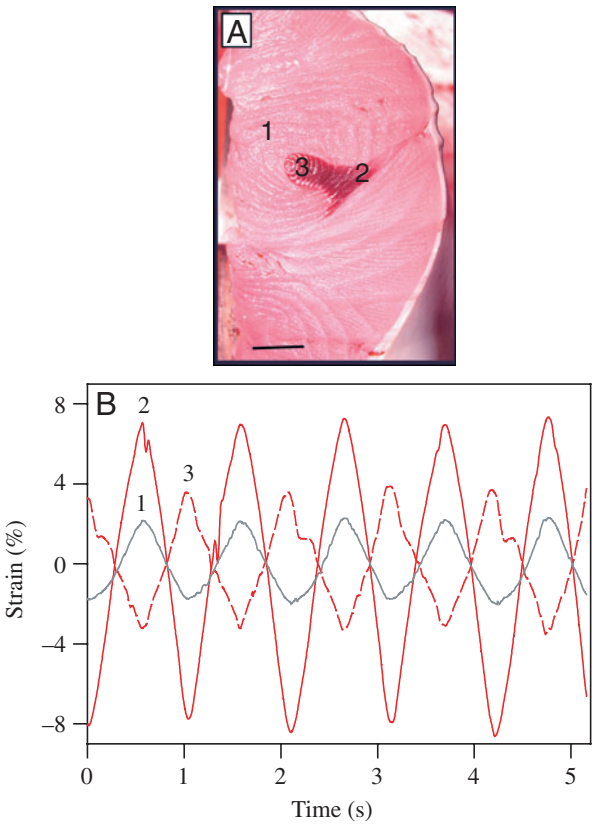

Fig. 8. Patterns of red (red traces) and white (gray trace) muscle strain at 0.6*L* during active swimming, illustrating variation in amplitude and phase of strain within the RM mass. The locations of implanted sonomicrometric crystals are indicated as numbers 1–3 in the body cross-section in A and correspond to the data traces in B. Scale bar, 1 cm.

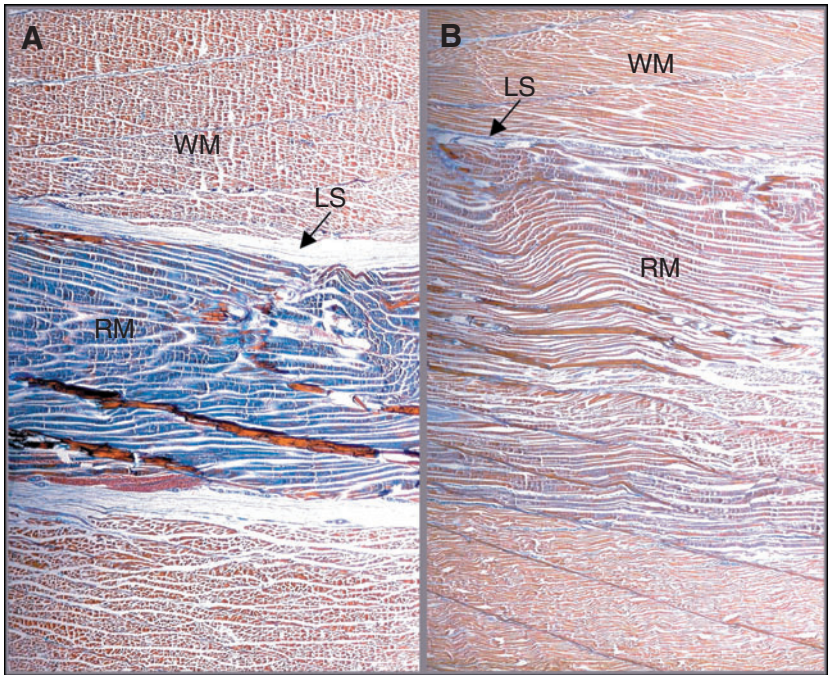

Fig. 9. Vertical parasagittal histological sections of medial (A) and lateral (B) edges of red muscle (RM) mass at 0.6*L*, illustrating the difference in development of lubricative sheath (LS). The lubricative sheath that surrounds the RM mass is thicker and more well-developed on the medial surface of the RM. Scale bar, 0.2 cm. WM, white muscle.

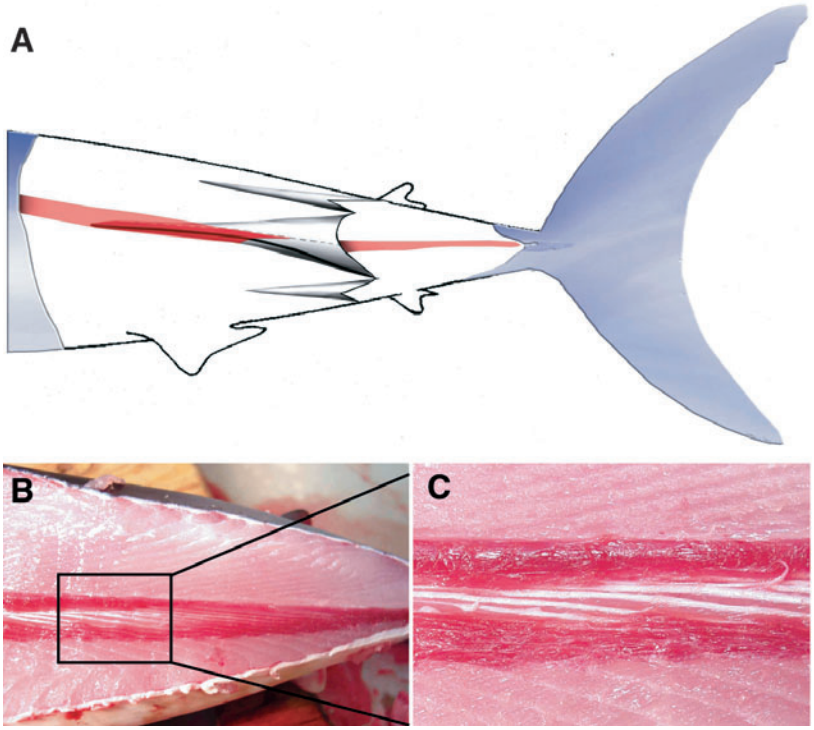

Fig. 10. Myotendinous architecture of the posterior region in the mako. (A) Diagram illustrating the myoseptal sheet (gray shaded region) and the relative position of the band of red muscle (RM; red) and hypaxial lateral tendon (black line); anterior to left. (B) Longitudinal section of RM (anterior to left; length of box is 5 cm), showing increase in hypaxial lateral tendon lengths (white) along the body. Enlarged image in C.

the RM mass where the surrounding lubricative sheath, the layer of smooth connective tissue that surrounds the RM mass, thought to facilitate shearing between the adjacent RM and WM, is more prominent (Fig. 9). Furthermore, peaks in WM strain preceded peaks in medial RM strain by nearly 50% of the strain cycle in this posterior position but were in phase with shortening in the peripheral RM (Fig. 8B). Thus, although strains in the WM and the most peripheral RM were in phase, their amplitudes differed, reflecting the general increase in strain that occurs away from the neutral axis of bending if the body deforms as a simple beam (Katz et al., 1999). This result suggests that moving from the medial edge to the periphery of the RM mass, strains vary in both magnitude and phase and that closest to the medial surface of the RM mass, where the lubricative sheath is most well-developed, RM strain is the most uncoupled from shortening of the surrounding musculature.

Patterns of muscle activation

In teleosts, a rostrocaudal decrease in duty cycle and a phase advance in EMG onset relative to the muscle strain cycle typically occur, a consequence of the activation wave traveling posteriorly at a higher speed than the wave of muscle contraction (Ellerby and Altringham, 1999). Changes in activation timing can have a significant effect on the net work and power produced by a muscle (Johnson and Johnston, 1991; Rome et al., 1993); thus, many studies have concluded that the longitudinal phase shift in activation timing leads to regional variation in muscle function in bony fishes (Altringham and Ellerby, 1999; Coughlin, 2000). Furthermore, changes in intrinsic contractile properties of muscle fibers along the body have been documented in many species; these also contribute to regional variation in muscle function during swimming (Coughlin, 2002). One exception to this general pattern is found in tunas that display no significant longitudinal variation in the phase of activation or muscle function of the deep RM between 0.4 and 0.74*L* (Shadwick et al., 1999; Syme and Shadwick, 2002), although duty cycles decrease posteriorly (Knower et al., 1999) and some regional variation in RM contractile properties have been reported (Altringham and Block, 1997; Syme and Shadwick, 2002). In eels, a posterior directed phase advance in RM activation occurs, but there is no significant difference in duty cycles or muscle power output as a function of axial position (D'Aout et al., 2001).

In a previous study, we found that, in contrast to teleosts, in the leopard shark both muscle activation phase and duty cycle remain constant along the body (Donley and Shadwick, 2003), and we hypothesized that regional variation in muscle function is not necessary for undulatory aquatic locomotion and may not occur in cartilaginous fishes. The muscle activation data presented here for the mako further support this hypothesis. In the mako, as in most fishes studied previously (Gillis, 1998; Altringham and Ellerby, 1999), onset of RM activation occurred during muscle lengthening and offset occurred during shortening (Fig. 2). However, both the phase and duration of activation remained constant along the body in the mako.

The present study identified one key difference in RM dynamics between mako and leopard sharks: mean onset and offset of activation occur approximately 30° later in the strain cycle in the mako, producing only a very short period in which the muscle is active while lengthening at both axial positions (Fig. 2). This significantly later activation phase suggests that RM in the mako may be faster to develop force and faster to relax than RM in the leopard shark. If so, then these fibers may perform proportionally less negative work and more net positive work in each contraction cycle. Since shorter activation and relaxation times allow muscle fibers to produce power at higher cycle frequencies, the mako may have a greater range of aerobic swimming speeds than its ectothermic relatives, as do tuna (Syme and Shadwick, 2002).

Another consequence of the relatively late activation of RM in the mako is that there is virtually no time during which posterior fibers perform negative work (i.e. active while lengthening) while anterior fibers actively shorten. In the leopard shark, by contrast, active lengthening of the mid and posterior muscle coincides with active shortening in the anterior for about 10% of each tailbeat cycle (Donley and Shadwick, 2003). During this time, the posterior fibers may develop high force and act to stiffen the body, facilitating power transmission from the anterior muscle along the body to the tail, as has been hypothesized for some teleosts (Altringham et al., 1993). Many bony fishes display even greater periods of simultaneous active lengthening in the posterior and positive power production in the anterior due to their characteristic rostrocaudal negative phase shift in muscle activation as well as the time delay in the strain wave as it travels along the body (Wardle et al., 1995; Altringham and Ellerby, 1999).

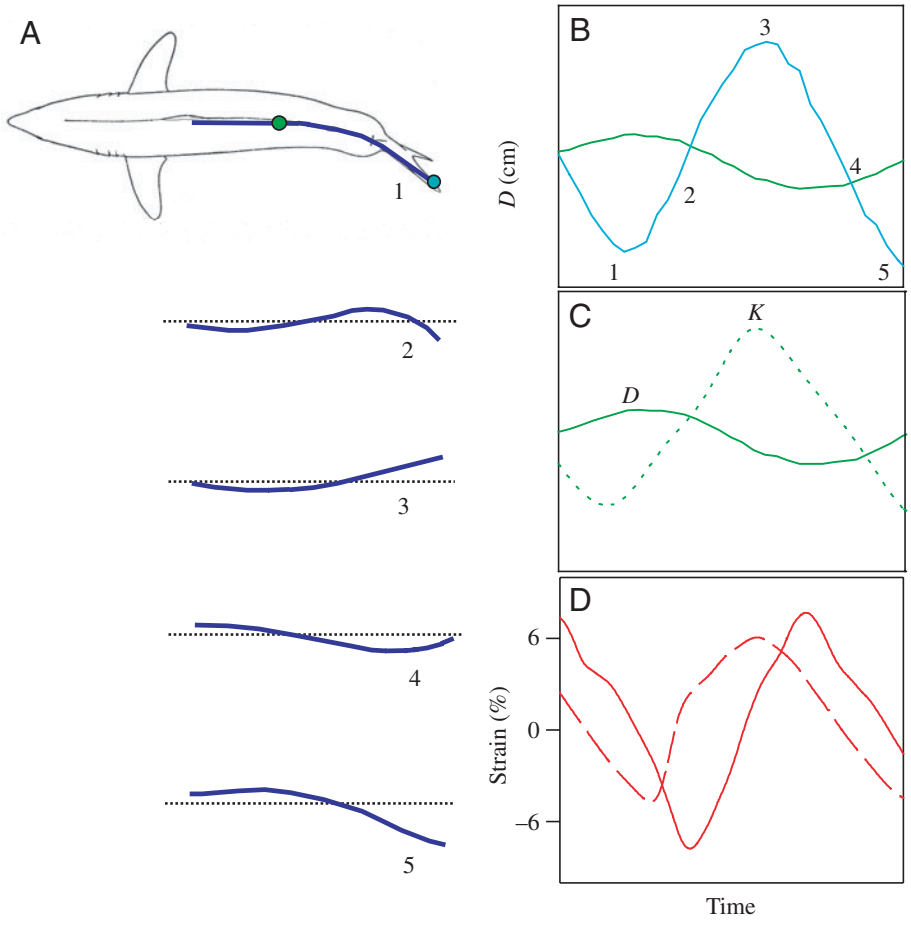

Fig. 11. Correlation between body kinematics and red muscle (RM) dynamics during steady swimming. (A) Dorsal midline traces from 0.4*L* to the tail tip (1.0*L*) for selected time intervals through one complete tailbeat cycle in an 87 cm *L* mako. Numbers indicate points in time as the tailbeat cycle progresses; dots indicate positions along the body (green is 0.6*L*, aqua is 1.0*L*) for which data are illustrated in B and C. (B) Lateral displacement (*D*) as a function of time for the tailbeat cycle shown in A. (C) Curvature (*K*) calculated at 0.6*L* (dotted line) superimposed on lateral displacement for 0.6*L* (solid line as in B) for the single tailbeat cycle. (D) RM strain for ~0.4*L* (broken red line) and ~0.6*L* (solid red line) on the left side of the body.

Because RM activation is so late in the mako, the period in which the muscle is active while lengthening is brief and there is no opportunity for posterior muscle fibers to act as force transmitters. Instead, we expect muscle function to be uniform along the body, with contractions optimized for positive power production, as has been shown to occur in tunas (Shadwick et al., 1999). Furthermore, strain amplitudes approximately double while RM cross-sectional area decreases by ~50% between 0.4 and 0.6*L* (Bernal et al., 2003), so we predict that overall work per cycle is similar at the two axial positions.

Most fishes generally bear a set of six intermuscular tendons within a single myoseptum (Gemballa et al., 2003). In the mako, one tendon out of this set of six, the hypaxial lateral tendon, shows striking differences to its homologue in bony fishes. This tendon is remarkably thick and elongated, up to 0.19*L* in the

posterior (Donley et al., 2004; Fig. 10), whereas the length of the homologous tendon in bony fishes at 0.6*L* does not exceed 0.075*L* (Gemballa and Treiber, 2003; Gemballa and Röder, 2004). Observed differences in tendon ultrastructure add further support to the idea that intermuscular tendons, not the muscle itself, are used for force transmission along the body in the mako.

Kinematics

In a previous study on the evolutionary convergence between lamnid sharks and tunas, we reported that lamnids swim more like tunas than like other sharks or subcarangiform teleosts (Donley et al., 2004). Lamnids share the same thunniform swimming mode, exemplified by a combination of minimal lateral motion in the mid-body region, where the bulk of the muscle resides, and reduced body mass in the caudal region, where lateral amplitudes are high (Donley et al., 2004). The present study provides additional kinematic data to show the strong similarity between lamnids and tunas. Specifically, we examined the degree of lateral displacement and curvature along the body and the relationship between the timing of waves of midline curvature, predicted strain and measured RM strain. Lateral displacement and midline curvature increase rostrocaudally (Fig. 6), but both have significantly lower amplitudes in the mako than in the leopard shark, between 0.4 and 0.8*L* (Fig. 7), indicating that the lamnid has a less undulatory mode of locomotion.

A defining characteristic of thunniform locomotion is the physical uncoupling of RM shortening from local body bending during steady swimming. This relationship between the timing of shortening in the deep RM and deformation of the surrounding tissue and skin was quantified in a number of ways in the mako. First, we found in all individuals that the timing of waves of predicted strain and curvature preceded measured RM strain. This phase relationship indicates that RM shortening is not linked to local bending but is, in fact, in phase with and thus influencing bending at more posterior body locations. This is illustrated in Fig. 3, which shows RM strain at 0.42*L* in phase with curvature calculated simultaneously at 0.6*L*. Second, we found that shortening in the RM and local WM at both axial positions was in phase when we imposed whole body undulations on inactive fish (i.e. ‘passive swimming’; Figs 4, 5). However, during steady swimming, shortening in the active RM was delayed relative to the adjacent white muscle by 10–17% of the tailbeat cycle in the anterior (Fig. 4), and this phase delay increased to nearly half of the tailbeat cycle in the posterior (Fig. 5). Thus, the RM shortening projects posteriorly along the mako, and the increase in the phase shift between shortening in the RM and local WM accords well with the rostrocaudal increase in myotomal lengths as well as the increase in hypaxial lateral tendon lengths recorded previously in the mako (Fig. 10; Donley et al., 2004).

In the leopard shark, as in most fishes with superficial RM, it has been shown that shortening in muscle occurs in phase with local body bending (Coughlin et al., 1996; Shadwick et al., 1998; Katz et al., 1999; Katz, 2002; Donley and Shadwick, 2003). The results presented here for the mako thus differ from the leopard shark and accord well with patterns observed in skipjack tuna, where Shadwick et al. (1999) reported that shortening in the deep RM occurred 17% later in the strain cycle than that predicted by midline curvature.

How do patterns of RM shortening along the body relate to whole-body kinematics in the mako? Fig. 11 illustrates the connection between the position of the dorsal midline and amplitudes of lateral displacement, body curvature and anterior and posterior RM strain as a function of time through one complete tailbeat cycle in an 87 cm *L* mako. During the course of a typical tailbeat cycle in a steady swimming mako, contractions of the body musculature produce a wave of lateral displacement that travels down the body rostrocaudally such that peaks in lateral displacement occur later in time at more posterior body positions. Fig. 11B compares the amplitudes of lateral displacement measured simultaneously at 0.6*L* and 1.0*L* (tail tip). As in most fish, the amplitude of lateral displacement in the mako increases towards the tail. In the mako, peaks in lateral displacement at 0.6*L* occur almost in synchrony with peaks in displacement at the tail tip but in the opposite direction. That is, when the tail tip is at its maximum in one direction, lateral displacement at 0.6*L* is at its maximum in the opposing direction. Curvature waves also propagate down the body from snout to tail but, unlike lateral displacement, the speed of the wave of *K* is much greater and increases rostrocaudally (Fig. 6). RM strain at 0.4*L* is in phase with *K* at 0.6*L*, as well as with peaks in displacement at the tail tip (Figs 3, 11B,C). Following the progress of muscle shortening at 0.4*L* (Fig. 11D), muscle on the left side of the body is lengthening at 0.4*L* when *K* is increasing and lateral displacement of the tail tip is increasing to the right. The RM at 0.4*L* therefore transmits its force down the body, causing bending at 0.6*L*, pulling the body at 0.6*L* and beyond to the left. This demonstrates that the RM in the mid-body region operates in near synchrony with the movements of the tail and is therefore uncoupled from local body curvature. Thus, by this uncoupling of RM shortening and local body bending, made possible by the development of thick and elongated hypaxial lateral tendons, the mako is able to achieve a tuna-like thunniform swimming mode (Donley et al., 2004).

Conclusion

Examination of the longitudinal patterns of RM strain and activation, together with dorsal midline kinematics, in a lamnid shark species, the shortfin mako (*Isurus oxyrinchus*), has demonstrated some key features of the locomotor system in makos that are in common with tunas as well as other sharks. One specific goal of this project was to test the hypothesis that the lack of longitudinal variation in the EMG/strain phase relationship is a characteristic consistent among sharks regardless of their mode of body/caudal fin propulsion. In support of this hypothesis, we found no variation in the timing of RM activation along the body in the mako and infer that functional properties of the RM remain constant from anterior

to posterior, a characteristic consistent with the leopard shark but unlike that observed in many bony fish species. As in tunas, the elongated tendons in the mako help transfer force along the body such that shortening in the RM is synchronous with bending at more posterior regions, a characteristic of thunniform locomotion.

The authors thank G. Lauder for providing software used to analyse body kinematics. Financial support was provided by NSF, The Scripps Graduate Department, and the San Diego ARCS Foundation.

References

Altringham, J. D. and Block, B. A. (1997). Why do tuna maintain elevated slow muscle temperatures? Power output of muscle isolated from endothermic and ectothermic fish. *J. Exp. Biol*. **200**, 2617-2627.

Altringham, J. D. and Ellerby, D. J. (1999). Fish swimming: Patterns in muscle function. *J. Exp. Biol*. **202**, 3397-3403.

Altringham, J. D. and Johnston, I. A. (1990). Modelling muscle power output in a swimming fish. *J. Exp. Biol.* **148**, 395-402.

Altringham, J. D., Wardle, C. S. and Smith, C. I. (1993). Myotomal muscle function at different locations in the body of a swimming fish. *J. Exp. Biol.* **182**, 191-206.

Bernal, D., Sepulveda, C. A., Mathieu-Costello, O. and Graham, J. B. (2003). Comparative studies of high performance swimming in sharks I. Red muscle morphometrics, vascularization and ultrastructure. *J. Exp. Biol*. **206**, 2831-2843.

Biewener, A. A. and Gillis, G. B. (1999). Dynamics of muscle function during locomotion: accommodating variable conditions *J. Exp. Biol*. **202**, 3387-3396.

Compagno, L. J. V. (1998). The living marine resources of the western central Pacific. In *FAO Identification Guide for Fishery Purposes* (ed. K. E. Carpenter and V. H. Niem), pp. 1274-1278. Rome: FAO.

Coughlin, D. J. (2000). Power production during steady swimming in largemouth bass and rainbow trout. *J. Exp. Biol.* **203**, 617-629.

Coughlin, D. J. (2002). Aerobic muscle function during steady swimming in fish. *Fish Fish.* **3**, 63-78.

Coughlin, D. J. and Rome, L. C. (1996). The roles of pink and red muscle in powering steady swimming in scup, *Stenotomus chrysops. Am. Zool.* **36**, 666-677.

Coughlin, D. J., Valdes, L. and Rome, L. C. (1996). Muscle length changes during swimming in scup: Sonomicrometry verifies the anatomical high-speed cine technique. *J. Exp. Biol.* **199**, 459-463.

D'Aout, K., Curtin, N. A., Williams, T. L. and Aerts, P. (2001). Mechanical properties of red and white swimming muscles as a function of the position along the body of the eel *Anguilla anguilla*. *J. Exp. Biol.* **204**, 2221-2230.

Donley, J. M. and Shadwick, R. E. (2003). Steady swimming muscle dynamics in the leopard shark *Triakis semifasciata*. *J. Exp. Biol*. **206**, 1117-1126.

Donley, J. M., Sepulveda, C. A., Konstantinidis, P., Gemballa, S. and Shadwick, R. E. (2004). Convergent evolution in mechanical design of lamnid sharks and tunas. *Nature* **429**, 61-65.

Ellerby, D. J. and Altringham, J. D. (2001). Spatial variation in fast muscle function of the rainbow trout *Oncorhynchus mykiss* during fast-starts and sprinting. *J. Exp. Biol.* **204**, 2239-2250.

Ellerby, D. J., Altringham, J. D., Williams, T. and Block, B. A. (2000). Slow muscle function of pacific bonito (*Sarda chiliensis*) during steady swimming. *J. Exp. Biol.* **203**, 2001-2013.

Gemballa, S. and Röder, K. (2004). From head to tail: The myoseptal system in basal actinopterygians. *J. Morphol.* **259**, 155-171.

Gemballa, S. and Treiber, K. (2003). Cruising specialists and accelerators – Are different types of fish locomotion driven by differently structured myosepta? *Zoology* **106**, 203-222.

Gemballa S., Ebmeyer L., Hagen K., Hoja K., Treiber K., Vogel F. and Weitbrecht, G. W. (2003). Evolutionary transformations of myoseptal tendons in gnathostomes. *Proc. R. Soc. London B Biol. Sci.* **270**, 1229-1235.

Gillis, G. (1998). Neuromuscular control of anguilliform locomotion: patterns of red and white muscle activity during swimming in the American eel *Anguilla rostrata*. *J. Exp. Biol*. **201**, 3245-3256.

Graham, J. B., Dewar, H., Lai, N. C., Lowell, W. R. and Arce, S. M. (1990). Aspects of shark swimming performance determined using a large water tunnel. *J. Exp. Biol.* **151**, 175-192.

Grillner, S. and Kashin, S. (1976). On the generation and performance of swimming in fish. In *Neural control of locomotion* (ed. R. M. Herman, S. Grillner, P. S. G. Stein and D. G. Stuart), pp. 181-201. New York: Plenum Press.

Hammond, L., Altringham, J. D. and Wardle, C. S. (1998). Myotomal slow muscle function of rainbow trout *Oncorhynchus mykiss* during steady swimming. *J. Exp. Biol.* **201**, 1659-1671.

He, P., Wardle, C. S. and Arimoto, T. (1990). Electrophysiology of the red muscle of mackerel, *Scomber scombrus* and its relation to swimming at low speeds. In *The 2nd Asian Fisheries Forum* (ed. R. Hirano and I. Hanyu), pp. 469-472. Manila: Asian Fisheries Society.

Hess, F. and Videler, J. J. (1984). Fast continuous swimming of saithe (*Pollachius virens*): A dynamic analysis of bending movements and muscle power. *J. Exp. Biol.* **109**, 229-251.

Jayne, B. C. and Lauder, G. V. (1993). Red and white muscle activity and kinematics of the escape response of the bluegill sunfish during swimming. *J. Comp. Physiol.* A. **173**, 495-508.

Jayne, B. C. and Lauder, G. V. (1995). Red muscle motor patterns during steady swimming in largemouth bass: Effects of speed and correlations with axial kinematics. *J. Exp. Biol.* **198**, 1575-1587.

Johnson, T. P. and Johnston, I. A. (1991). Power output of fish muscle fibres performing oscillatory work: effects of acute and seasonal temperature change. *J. Exp. Biol*. **157**, 409-423.

Katz, S. L. (2002). Design of heterothermic muscle in fish. *J. Exp. Biol*. **205**, 2251-2266.

Katz, S. L. and Shadwick, R. E. (1998). Curvature of swimming fish midlines as an index of muscle strain suggests swimming muscle produces net positive work. *J. Theor. Biol.* **193**, 243-256.

Katz, S. L., Shadwick, R. E. and Rapoport, H. S. (1999). Muscle strain histories in swimming milkfish in steady and sprinting gaits. *J. Exp. Biol*. **202**, 529-541.

Katz, S. L., Syme, D. A. and Shadwick, R. E. (2001). Enhanced power in yellowfin tuna. *Nature* **410**, 770-771.

Knower, T., Shadwick, R. E., Katz, S. L., Graham, J. B. and Wardle, C. S. (1999). Red muscle activation patterns in yellowfin and skipjack tunas during steady swimming. *J. Exp. Biol.* **202**, 2127-2138.

Rome, L. C. and Swank, D. (1992). The influence of temperature on power output of scup red muscle during cyclic length changes. *J. Exp. Biol.* **171**, 261-282.

Rome, L. C., Funke, R. P. and Alexander, R. M. (1990). The influence of temperature on muscle velocity and sustained performance in swimming carp. *J. Exp. Biol.* **154**, 163-178.

Rome, L. C., Sosnicki, A. and Choi, I. H. (1992). The influence of temperature on muscle function in the fast swimming scup. 2. The mechanics of red muscle. *J. Exp. Biol.* **163**, 281-295.

Rome, L. C., Swank, D. and Corda, D. (1993). How fish power swimming. *Science* **261**, 340-343.

Shadwick, R. E., Steffensen, J. F., Katz, S. L. and Knower, T. (1998). Muscle dynamics in fish during steady swimming. *Amer. Zool.* **38**, 755-770.

Shadwick, R. E., Katz, S. L., Korsmeyer, K. E., Knower, T. and Covell, J. W. (1999). Muscle dynamics in skipjack tuna: timing of red muscle shortening in relation to activation and body curvature during steady swimming. *J. Exp. Biol.* **202**, 2139-2150.

Syme, D. A. and Shadwick, R. E. (2002). Effects of longitudinal body positions and swimming speed in mechanical power of deep red muscle from skipjack tuna (*Katsuwonus pelamis*). *J. Exp. Biol.* **205**, 189-200.

van Leeuwen, J. L., Lankheet, M. J. M., Akster, H. A. and Osse, J. W. M. (1990). Function of red axial muscles of carp (*cyprinus-carpio*): recruitment and normalized power output during swimming in different modes. *J. Zool.* **220**, 123-145.

Wardle, C. S. and Videler, J. J. (1993). The timing of the electromyogram in the lateral myotomes of mackerel and saithe at different swimming speeds. *J. Fish Biol.* **42**, 347-359.

Wardle, C. S., Videler, J. J. and Altringham, J. D. (1995). Tuning in to fish swimming waves: Body form, swimming mode and muscle function. *J. Exp. Biol.* **198**, 1629-1636.

Williams, T. L., Grillner, S., Smoljaninov, V. V., Wallen, P., Kashin, S. and Rossignol, S. (1989). Locomotion in lamprey and trout: the relative timing of activation and movement. *J. Exp. Biol.* **143**, 559-566.